Available online at www.sciencedirect.com
ScienceDirect
Advances in Space Research 46 (2010) 144–149
ADVANCES IN SPACE RESEARCH (a COSPAR publication)
www.elsevier.com/locate/asr

Cycle slip detection using multi-frequency GPS carrier phase observations: A simulation study

Y. Wu [a,*], S.G. Jin [b], Z.M. Wang [c], J.B. Liu [c]

[a] Key Laboratory of Geological Hazards, University of Three Gorges, 3 Daxue Road, Yichang 443002, China
[b] Shanghai Astronomical Observatory, Chinese Academy of Sciences, 80 Nandan Road, Shanghai 200030, China
[c] School of Geodesy and Geomatics, Wuhan University, 129 Luoyu Road, Wuhan 430079, China

Received 7 August 2009; received in revised form 10 November 2009; accepted 11 November 2009

Abstract

The detection and repair of the cycle slip or gross error is a key step for high precision global positioning system (GPS) carrier phase navigation and positioning due to interruption or unlocking of GPS signal. A number of methods have been developed to detect and repair cycle slips in the last two decades through cycle slip linear combinations of available GPS observations, but such approaches are subject to the changing GPS sampling and complex algorithms. Furthermore, the small cycle slip and gross error cannot be completely repaired or detected if the sampling is quite longer under some special observation conditions, such as Real Time Kinematic (RTK) positioning. With the development of the GPS modernization or Galileo system with three frequencies signals, it may be able to better detect and repair the cycle slip and gross error in the future. In this paper, the cycle slip and gross error of GPS carrier phase data are detected and repaired by using a new combination of the simulated multi-frequency GPS carrier phase data in different conditions. Results show that various real-time cycle slips are completely repaired with a gross error of up to 0.2 cycles.

Keywords: GPS; Cycle slip; Gross error; Multi-frequency combination

1. Introduction

High quality GPS carrier phase observations play a key role in high precision GPS static or kinematic positioning. However, due to internal tracking problems of GPS receiver or signal interruption of the antenna from the satellite, the continuous original carrier phase observations are destroyed, namely generating cycle slips and gross errors (Seeber, 1993), which directly affect GPS positioning results. Therefore, accurately detecting and repairing the gross errors and cycle slips is an important pre-processing step in high precision GPS carrier phase positioning and applications (Jin et al., 2006). Traditional detection methods are based on the gross error theory that the cycle slips are detected as obvious gross errors from the GPS carrier phase measurement time series. The remaining residuals as a random part are much less than the minimal cycle slip. In practice, it is very difficult to accurately detect and repair the small cycle slip in original GPS carrier phase measurements because of the clock error, atmospheric refraction delay and multi-path effect (Jin et al., 2005), especially for Real Time Kinematic (RTK) GPS positioning. In the past two decades, many approaches have been developed to detect and repair the cycle slip in the GPS carrier phase static and kinematic positioning. For examples, the big cycle slips can be detected by the polynomial fitting method or high-order differentiation, and then the smaller cycle is detected and repaired from the residuals, e.g. using Kalman filtering technique (Bastos and Landau, 1988). Lu and Lachapelle (1992) developed the DIA (Detection, Identification and Adaptation) algorithm to search multiple cycle slips simultaneously using two-step Kalman filtering. Han (1997) developed a combination method of ambiguity

* Corresponding author. Tel.: +86 21 64386191; fax: +86 21 64384618.
E-mail addresses: wu_gps@yahoo.com (Y. Wu), sgjin@shao.ac.cn (S.G. Jin).

0273-1177/$36.00 © 2009 COSPAR. Published by Elsevier Ltd. All rights reserved.
doi:10.1016/j.asr.2009.11.007

function with Kalman filtering technique, and so on. However, all above methods must use many epochs of GPS observations with a low sampling and complicated algorithms as well as post-processing. Moreover, as the difference observations are used, it is not able to detect the real-time cycle slips and gross errors for the original GPS carrier phase measurements. Therefore, detecting and repairing cycle slips and gross errors is still a challenge for the high precision GPS carrier phase positioning even with a long time observation.

With the development of multi-frequency GPS signals, such as extending a third civil signal (1176.45 MHz, L_5) in the GPS Modernization and Galileo navigation system, it may improve the cycle slip detection and repair through multi-frequency carrier phase observation combinations. In this paper, the cycle slip detection and repair are investigated and evaluated through using a new combination of the simulated multi-frequency GPS carrier phase observations in different conditions.

2. Simulation of multi-frequency GPS carrier phase observations

Although dual-frequency GPS code and carrier phase observations have lots of errors, but the ionospheric delay is related to the frequency, the tropospheric delay and clock offset are equal at the same epoch for different frequency, and multi-path and stochastic noises are independent. Therefore, some errors can be mitigated or removed through a certain combination of dual-frequency GPS observations. In contrast, the third frequency data can be simulated through their error relations (Wu, 2005). Here the frequency 1176.45 MHz is used as the third civil signal, coinciding with the L_5 in the GPS Modernization or Galileo navigation system. Fig. 1 shows the GPS carrier phase observations φ_1^t, φ_2^t and φ_5^t for L_1, L_2 and L_5 at epoch t_i ($i = 1, 2$), respectively. GPS observation equations for L_1 carrier phase at epoch t_1 and t_2 can be written:

$$\lambda_1\varphi_1^{t_1} + \lambda_1 N_1 = \rho^{t_1} + c(\delta t_r^{t_1} - \delta t^{jt_1}) + \Delta I_1^{t_1} + \Delta T_1^{t_1} + \varepsilon_1^{t_1} \quad (1)$$

$$\lambda_1\varphi_1^{t_2} + \lambda_1 N_1 = \rho^{t_2} + c(\delta t_r^{t_2} - \delta t^{jt_2}) + \Delta I_1^{t_2} + \Delta T_1^{t_2} + \varepsilon_1^{t_2} \quad (2)$$

where λ_1 is the carrier phase wavelength, $c(\delta t_r^{t_i} - \delta t^{jt_i})$, $\Delta I_1^{t_i}, \Delta T_1^{t_i}$ and $\varepsilon_1^{t_i}$ are clock offset difference between receiver and satellite, ionospheric delay, tropospheric delay and noise, respectively, N is the carrier phase ambiguity. The observation equation between epoch t_1 and t_2 can be written from Eqs. (1) and (2):

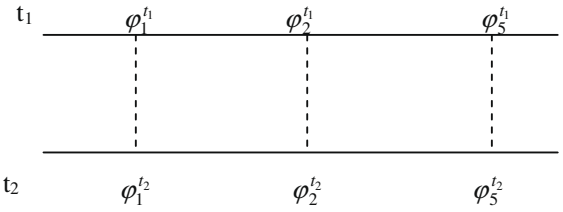

Fig. 1. Sketch map of each frequency phase between tow epochs.

$$\lambda_1(\varphi_1^{t_2} - \varphi_1^{t_1}) = (\rho^{t_2} - \rho^{t_1}) + c\Delta\delta^{t_2-t_1} + \Delta I_1^{t_2-t_1} + \Delta T_1^{t_2-t_1} + \Delta\varepsilon_1^{t_2-t_1} \quad (3)$$

At the similar way, the equations for L_2 and L_5 between epoch t_1 and t_2 are obtained as:

$$\lambda_2(\varphi_2^{t_2} - \varphi_2^{t_1}) = (\rho^{t_2} - \rho^{t_1}) + c\Delta\delta^{t_2-t_1} + \Delta I_2^{t_2-t_1} + \Delta T_2^{t_2-t_1} + \Delta\varepsilon_2^{t_2-t_1} \quad (4)$$

$$\lambda_5(\varphi_5^{t_2} - \varphi_5^{t_1}) = (\rho^{t_2} - \rho^{t_1}) + c\Delta\delta^{t_2-t_1} + \Delta I_5^{t_2-t_1} + \Delta T_5^{t_2-t_1} + \Delta\varepsilon_5^{t_2-t_1} \quad (5)$$

As the receiver clock offset $c\delta t_r^t$, satellite clock offset $c\delta t^{jt_i}$, tropospheric delay ΔT^t and geometrical distance ρ are equal for the same GPS satellite at one station, the differences between Eqs. (3) and (4) or (5) can be written as:

$$\lambda_1\Delta\varphi_1 - \Delta I_1^{t_2-t_1} = \lambda_i\Delta\varphi_i - \Delta I_i^{t_2-t_1} \quad (6)$$

where $\Delta\varphi_i = \varphi_i^{t_2} - \varphi_i^{t_1} (i = 2, 5)$. Eq. (6) can be further expressed as:

$$\Delta\varphi_i = (\lambda_1\Delta\varphi_1 - \Delta I_1^{t_2-t_1} + \Delta I_i^{t_2-t_1})/\lambda_i = \left[\lambda_1\Delta\varphi_1 - \left(1 - \frac{f_1^2}{f_i^2}\right)\Delta I_1^{t_2-t_1}\right]/\lambda_i \quad (7)$$

As the ionospheric delay can be obtained from dual-frequency GPS data, the difference for L_5 carrier phase observations at two epochs can be written as:

$$\Delta\varphi_5 = \frac{\lambda_1}{\lambda_5}\left[\Delta\varphi_1 - \left(1 - \frac{f_1^2}{f_5^2}\right)\left(\Delta\varphi_1 - \frac{f_1}{f_2}\Delta\varphi_2\right)\left(\frac{f_2^2}{f_2^2 - f_1^2}\right)\right] \quad (8)$$

Therefore, the observations for L_5 carrier phase at each epoch can be simulated based on Eq. (8), while the initial value at the first epoch is arbitrary.

3. Combination of multi-frequency GPS carrier phase observations

Three-frequency GPS carrier phase observation equations are as following:

$$L_1 = \lambda_1\varphi_1 = \rho - \lambda_1 N_1 + T + I + \delta r + m_1 + \varepsilon_1 \quad (9)$$

$$L_2 = \lambda_2\varphi_2 = \rho - \lambda_2 N_2 + T + q_1 I + \delta r + m_2 + \varepsilon_2 \quad (10)$$

$$L_5 = \lambda_5\varphi_5 = \rho - \lambda_5 N_5 + T + q_2 I + \delta r + m_5 + \varepsilon_5 \quad (11)$$

where λ_i is the carrier phase wavelength ($i = 1, 2$ and 5), N_i is the carrier phase ambiguity ($i = 1, 2$ and 5), T, I and δr are the tropspheric and ionospheric delay and arbitrary errors, respectively, m_i and ε_i are the multi-path error and noise ($i = 1, 2$ and 5), respectively, q_1 is $(\lambda_2/\lambda_1)^2$ and q_2 is $(\lambda_5/\lambda_1)^2$. So the multi-frequency carrier phase combination can be written:

$$\begin{aligned} L_c &= \alpha L_1 + \beta L_2 + \gamma L_5 \\ &= (\alpha + \beta + \gamma)\rho - (\alpha\lambda_1 N_1 + \beta\lambda_2 N_2 + \gamma\lambda_5 N_5) \\ &\quad + (\alpha + \beta + \gamma)(T + \delta r) + (\alpha + \beta q_1 + \gamma q_2)I \\ &\quad + (\alpha n_1 + \beta n_2 + \gamma n_5) + (\alpha m_1 + \beta m_2 + \gamma m_5) \end{aligned} \quad (12)$$

In order to make geometrical distance ρ not to be influenced by various combinations, we assume $\alpha+\beta+\gamma=1$, and therefore Eq. (12) can be written as

$$L_c = \rho - \lambda N + (T+\delta r) + \eta I + n_{L_c} + m_{L_c} \tag{13}$$

where $\lambda N = \alpha\lambda_1 N_1 + \beta\lambda_2 N_2 + \gamma\lambda_5 N_5$, $\eta = \alpha\lambda N + \beta q_1 + \gamma q_2$, $n_L = \alpha n_1 + \beta n_2 + \gamma n_5$, and $m_{L_c} = \alpha m_1 + \beta m_2 + \gamma m_5$. In order to keep the integer character of combination observations' ambiguity, i, j, and k, respectively should be the integer and then α, β *and* γ are respectively written as

$$\alpha = i\lambda/\lambda_1, \quad \beta = j\lambda/\lambda_2, \quad \gamma = k\lambda/\lambda_5 \tag{14}$$

Substituting Eq. (14) into $\alpha+\beta+\gamma=1$, the wavelength of combination observations can be expressed by

$$\lambda = \frac{\lambda_1\lambda_2\lambda_5}{i\cdot\lambda_2\lambda_5 + j\cdot\lambda_1\lambda_5 + k\cdot\lambda_1\lambda_2} \tag{15}$$

Assuming $\alpha_\lambda = \lambda/\lambda_5$, i.e. combination wavelength scale coefficient, it reflects the scale change of combination wavelength relative to λ_5. As the signal frequency f is c/λ, where c is the velocity of light, the frequency of combination observations can be written from Eq. (15):

$$f = if_1 + jf_2 + kf_3 \tag{16}$$

and multi-frequency carrier phase combination observation can be written as:

$$\varphi_{i,j,k} = i\varphi_1 + j\varphi_2 + k\varphi_3 \tag{17}$$

According to Eq. (15), long-wave combinations can be calculated. For example, Table 1 lists the part of long-wave combinations.

4. Method of cycle slips detection using pseudo-range/carrier phase combination

GPS pseudo-range and carrier phase observation equations can be written, respectively:

$$R = \rho + I_R + T_R + m_r + \varepsilon_r \tag{18}$$

$$\lambda\varphi = \rho + \lambda N + I_\varphi + T_\varphi + m_\varphi + \varepsilon_\varphi \tag{19}$$

where R is the pseudo-range observation, φ is the carrier phase observation, λ is the wavelength of carrier phase, N is the integer ambiguity, I_R and I_φ, T_R and T_φ, m_r and m_φ, ε_r and ε_φ are the ionospheric delay, tropospheric delay, multi-path error and noises of pseudo-range and carrier phase observations, respectively. Through the difference above two equations (18) and (19), the ambiguity can be written as

$$N = \frac{[\lambda\varphi - R - (I_\varphi - I_R) - (m_\varphi - m_R) - (\varepsilon_\varphi - \varepsilon_R)]}{\lambda} \tag{20}$$

The estimation of cycle slip can be determined via difference between epoch t_2 and t_1:

$$\Delta N = N(t_2) - N(t_1) = \varphi(t_2) - \varphi(t_1) - \frac{R(t_2) - R(t_1)}{\lambda} \tag{21}$$

From Eqs. (20) and (21), it can be seen that the precision of cycle slip estimation mainly relies on the change of ionospheric and multi-path errors between two epochs, the noise of pseudo-range and carrier phase observations, and the wavelength of carrier phase. Under the same observation condition, the longer wavelength has the higher precision of cycle slip estimation. For the current dual-frequency GPS observation combinations, the error correlation to the time will be enlarged with the increase of observation sampling, and therefore the ability of the traditional cycle slip detection will be greatly degraded.

Table 1
Combinations characters of long-wave combinations

i	j	k	f (MHz)	λ (m)	α_λ
−9	2	10	40.92	7.33	28.75
−3	1	3	30.69	9.77	38.33
−3	2	2	81.84	3.66	14.38
−1	8	−7	10.23	29.31	115.00
−1	9	−8	61.38	4.88	19.17
−1	10	−9	112.53	2.66	10.45
0	1	−1	51.15	5.86	23.00
1	−7	6	40.92	7.33	28.75
1	−6	5	92.07	3.26	12.78
3	0	−4	20.46	14.65	57.50
7	−8	−1	30.69	9.77	38.33
−7	9	0	20.46	14.65	57.50

5. Cycle slip detection using multi-frequency carrier phase combinations

5.1. Combination of multi-frequency carrier phase observations

Cycle slips can be amplified in long-wave observation combination when the original carrier phase observations have cycle slips. Given that the three groups of cycle slips in each original carrier phase observation between two epochs are N_1, N_2 and N_3, and the three-group combination cycle slips (n_1, n_2, n_3) can be written as $a_1N_1 + b_1N_2 + c_1N_3$, $a_2N_1 + b_2N_2 + c_2N_3$, $a_3N_1 + b_3N_2 + c_3N_3$, respectively, namely

$$\begin{cases} a_1N_1 + b_1N_2 + c_1N_3 = n_1 \\ a_2N_1 + b_2N_2 + c_2N_3 = n_2 \\ a_3N_1 + b_3N_2 + c_3N_3 = n_3 \end{cases} \tag{22}$$

According to the combination of multi-frequency carrier phase observation in Section 3, the three groups of long-wave uncorrelated combinations, $\varphi_{0,1,-1}$, $\varphi_{-3,1,3}$, $\varphi_{-1,8,-7}$, are chosen in this test, seeing Table 1. Here, the simulated third frequency observation data with the sampling of 15 s are used to evaluate the cycle slip detection.

The cycle slip detections of various combination conditions are investigated, such as small cycle slips (L_1-1, L_2-1) in Fig. 2a, (L_1-1, L_2-5) in Fig. 2b, and big cycle slips (L_1-60, L_2-130) in Fig. 2c. The detected values are then substituted into Eq. (22). Results show that the cycle slip for each original observation at each epoch can be correctly obtained. Fig. 3 shows various gross errors at levels

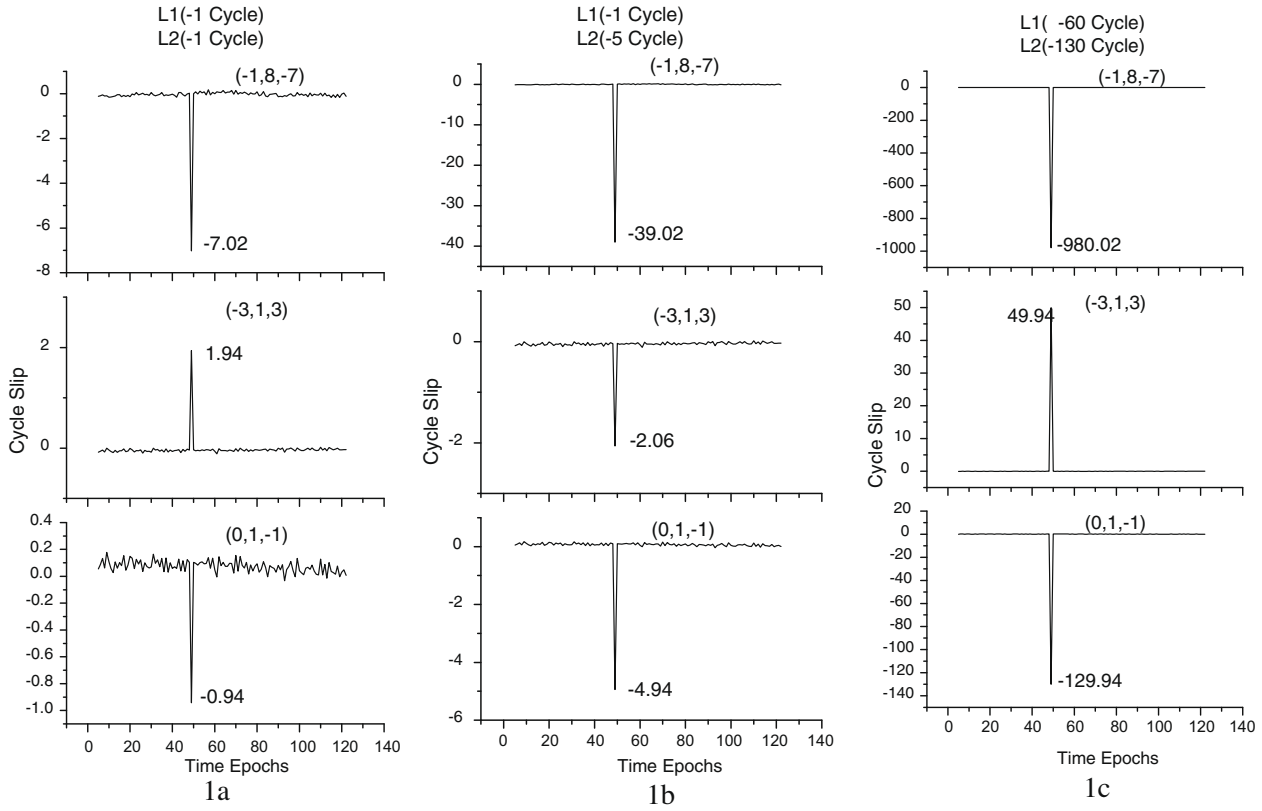

Fig. 2. Detection of various cycle slips using multi-frequency carrier phase combinations.

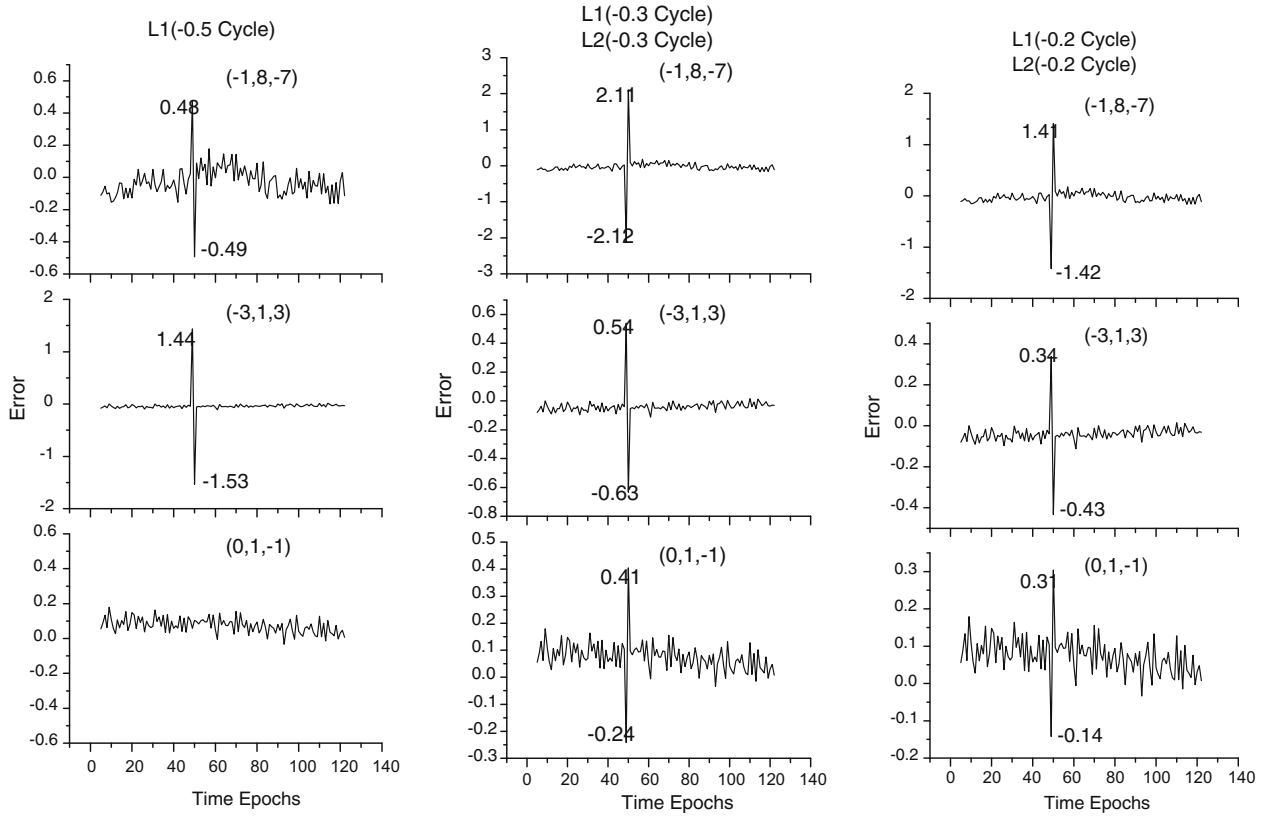

Fig. 3. Detection of various gross errors (cycle) using multi-frequency carrier phase combinations.

of 0.5, 0.3, and 0.2 cycles using multi-frequency carrier phase combinations. It can be seen that the gross error above 0.2 cycles is well detected. Even the sampling is 30 s and 60 s, and the gross error and cycle slip are still successfully detected and repaired.

5.2. Baseline cycle slip detection using multi-frequency carrier phase combinations

In order to further check the cycle slip detection capability using multi-frequency carrier phase combinations in Section 5.1, we tested a pair of GPS baseline, where one of GPS stations is under the slightly bad observation condition. Observation data of PRN20 are chosen to check the gross error in this test using the simulated third frequency data. Here the three groups of long-wave uncorrelated combinations, $\varphi_{0,1,-1}$, $\varphi_{3,0,-4}$, $\varphi_{-7,9,0}$, are used, seeing Table 1, as their combinations use only two frequency observations, and therefore it will easily check the gross errors at epochs of one by one. Figs. 4–6 show the test results of each combination, respectively. It has been seen that there is no gross error in the observation data of L_2–L_5 in Fig. 4, but there are obvious gross errors at some epochs for L_1 combinations with L_2 and L_5 (Fig. 5 and 6), respectively, indicating a gross error in L_1 carrier phase observations. This test shows that the quality of original

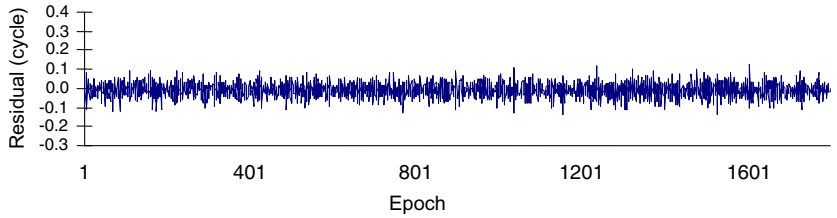

Fig. 4. Near-real-time gross errors detection (cycle) of the L_2–L_5 observations using pseudo-range/carrier phase combination (0, 1, −1).

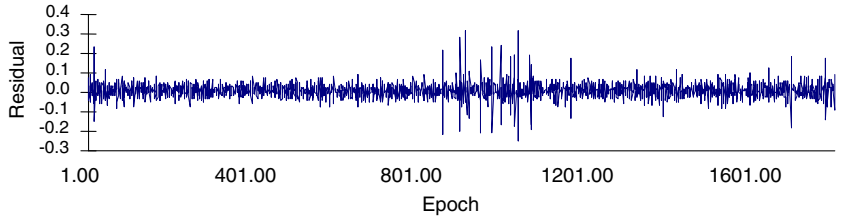

Fig. 5. Near-real time gross errors detection (cycle) of the L_1–L_5 observations using pseudo-range/carrier phase combination (3, 0, −4).

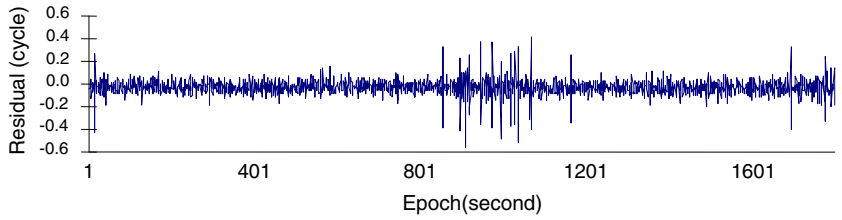

Fig. 6. Near-real time gross errors detection (cycle) of the L_1–L_2 observations using pseudo-range/carrier phase combination (−7, 9, 0).

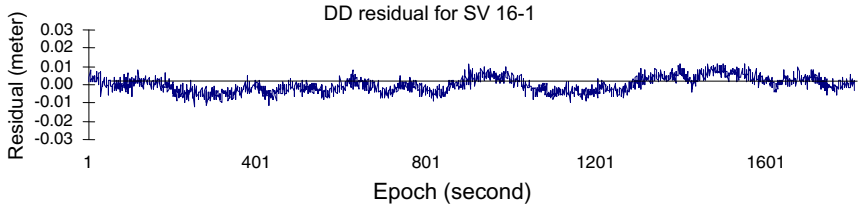

Fig. 7. The double-difference residuals (meter) of baseline for the satellite pair of PRN1-16.

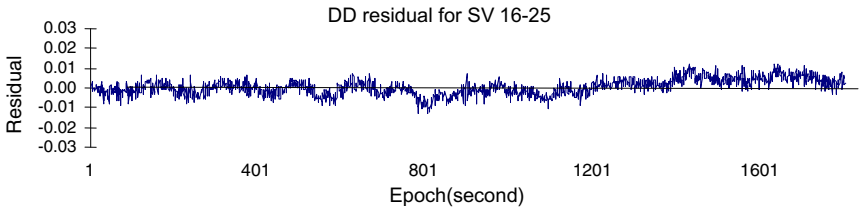

Fig. 8. The double-difference residuals (meter) of baseline for the satellite pair of PRN25-16.

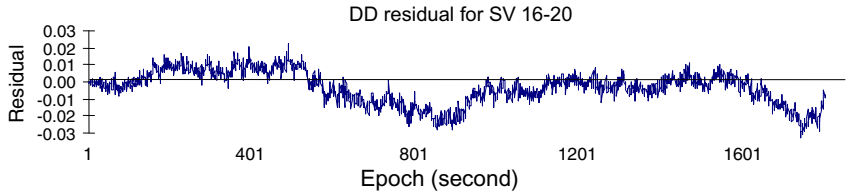

Fig. 9. The double-difference residuals (meter) of baseline for the satellite pair of PRN20-16.

GPS carrier phase observation can be real-timely checked using characters of multi-frequency carrier phase combinations.

In addition, to check the reliability of above tested results, the double-differenced observation residuals in L_1 are further calculated with respect to the reference satellite PRN16. Figs. 7 and 8 show the residuals of PRN1-16 and PRN25-16, respectively. It can be seen that qualities of PRN1 and PRN25 observations are quite good at amplitude of ± 1 cm. The larger residuals in PRN20 are found in Fig. 9 with amplitude of ± 3 cm at some epoch, which is consistent with Figs. 5 and 6 at the epoch of gross error detection. It again indicates the reliability and superiority using multi-frequency carrier phase observation combinations.

6. Conclusions

A new approach of cycle slips and gross errors detection for the original GPS carrier phase observation is presented using multi-frequency carrier phase combinations. Testing results show that the real-time cycle slip and gross error can be well detected and repaired under the long sampling condition with up to the level of 0.2 cycles. The baseline results also show a larger advantage that it is able to check the gross error for each original carrier phase observation at each epoch using three groups of uncorrelated dual-frequency observation combinations, and the residuals again prove the reliability and superiority of this method. In the future, it is needed to further test with real observation data.

References

Bastos, L., Landau, H. Fixing cycle slips in dual-frequency kinematic GPS-applications using Kalman filtering. Manuscr. Geod. 13, 249–256, 1988.

Han, S. Quality control issues relating to ambiguity resolution for real-time GPS kinematic positioning. J. Geod. 71 (6), 351–361, 1997.

Jin, S.G., Park, J., Wang, J., Choi, B., Park, P. Electron density profiles derived from ground-based GPS observations. J. Navig. 59 (3), 395–401, 2006.

Jin, S.G., Wang, J., Park, P. An improvement of GPS height estimates: stochastic modeling. Earth Planets Space 57 (4), 253–259, 2005.

Lu, G., Lachapelle, G. Statistical quality control for kinematic GPS positioning. Manuscr. Geod. 17, 270–281, 1992.

Seeber, G. Satellite Geodesy Foundations, Methods, and Applications. Berlin, New York, 1993.

Wu, Y. Multi-frequency GPS data modeling/processing and its applications. PhD Thesis, Wuhan University, 71–76, 2005.